Details of the Keck/OSIRIS Observations: The strongly-lensed z=3.07 galaxy, J2135-0102[1] was observed with OSIRIS[2] in conjunction with the Laser Guide Star Adaptive Optics system on the Keck II 10 metre telescope on UT September 4-5 2007 in photometric conditions and an optical seeing of 0.5 arcsec FWHM. The resulting Strehl is 25% and the encircled energy is 50% within a radius of 0.10 arcseconds. In order to map the nebular emission lines of [O III] λλ4959, 5007 Å and Hβ 4861 Å, we used the narrow band Kn1 filter which provides a wavelength coverage from 1.955 to 2.055μm at a spectral resolution of $\lambda/\Delta\lambda \sim 3400$. When deriving emission line widths, we subtract the instrumental profile, whose FWHM is 5.9×10^{-4} μm, in quadrature. As the target only partially fills the OSIRIS integral field unit (IFU) using the 0.1 arcsec lenslet scale, observations were conducted using a ABBA sequence with a 3.2 arcsec East-West chop onto adjacent sky, keeping the target within the field of view. The total integration time comprised 20 sub-exposures of 750 seconds. Individual exposures were reduced using the OSIRIS data reduction package. From each resulting datacube, a continuum image was constructed and the centroid of the foreground lensing galaxy measured. The final datacube was constructed by aligning the sub-exposures and combining using a 3σ clip to reject cosmic rays. Flux calibration was obtained by observing the R=14.2 `tip tilt' star prior to each observation.

Gravitational Lens Modelling: To interpret our data we must correct for the gravitational magnification and reconstruct the galaxy in the source plane. We first assign accurate world coordinates to each spectral pixel using the known coordinates of the foreground lens and the position angle of the IFU. The source plane is subsequently reconstructed with the

lens model held fixed to the parameterization determined using the high signal/noise HST data[3] taking care to account for the PSF of the OSIRIS observations.

We note that the variable magnification across J2135-0102 leads to non-uniform resolution in the source plane; however we take this into consideration during the source-plane reconstruction of the data cube by utilizing an adaptive source plane grid[4]. Regions in the image plane that are more highly magnified map to correspondingly smaller source plane pixels. The pixel size in each region of the source plane is selected by ray-tracing the image of the PSF into the source plane and ensuring that the derived resolution is finer than the pixel size. Hence each pixel in the source plane represents a nearly independent measurement of the intensity and velocity field. The pixel size ranges from 0.02 arcseconds in the regions of high magnification to 0.04 arcseconds in the regions of lower magnification, corresponding to physical scales of ~150 to 300 pc at z=3.07.

To evaluate the uncertainty on the magnification factor and on the image reconstruction, we also create a family of acceptable lens models. These models are constructed by varying the four main parameters of the lens model, namely the normalization of the dark matter halo density distribution of the lens galaxy, the elongation of the halo (the major / minor axis ratio), the orientation of the major axis, and the external shear provided by the cluster, such that the $\Delta\chi^2$ value from the best fit varies by $\pm 1\sigma$. Ray tracing each of these models and re-deriving the source-plane morphology and velocity field produces only minor changes in the dynamics, typically the various mappings produce a maximum shift of ~0.01 arcseconds compared to the best-fit solution and only a 10% uncertainty in the derived magnification (Supplementary Figure 1). All of the derived quantities in this paper include this uncertainty.

Analysis of Emission Line Maps: The distribution of velocities and line widths across J2135-0102 was computed by fitting the [O III] λ5007 emission line in the spectral direction at each spatial location with a flat continuum plus Gaussian emission line profile using a χ^2 minimization procedure which takes into account the greater noise level close to atmospheric OH emission. We demanded a minimum signal to noise ratio of 5 to detect the emission line, and when this criterion is met, we determine the centroid, flux and line width of the best fit. In regions where the fit failed to detect a line, we average the surrounding 2 × 2 pixels and attempt the fit again. To derive error bars on each parameter we perturb the best fit such that the $\Delta\chi^2$ value from the best fit varies by $\pm 1\sigma$.

Star formation rates are derived from the Hβ line fluxes following the Kennicutt calibration[5] which assumes a Salpeter IMF ranging from 0.1 to 100 solar masses and case B recombination. We rule out a significant contribution to the recombination flux from an active galactic nucleus (which would bias our star formation rate estimates) from the absence of bright CIV emission[1] and bright mid-IR continuum[6]. The integrated Hβ line flux implies a star formation rate of 40 solar masses / year. This value likely underestimates the star formation rate of J2135-0102 since it does not account for dust. If we adopt an extinction correction of A(Hβ)~1 mag, estimated by taking into account the reddening suggested from the broadband SED[6], the intrinsic star formation rate of J2135-0102 is closer to 100 solar masses / year. This is still consistent with the mid-infrared star formation rate[6] (60 solar masses / year) and is identical to that predicted from the extinction corrected rest-UV continuum[1].

Rotation vs. Merger Interpretation: Throughout the article, we argue that the most consistent explanation of our velocity and line width information (Figure 2) follows if the

galaxy has well-ordered rotation. Here we discuss whether other interpretations are possible. In particular, are the data consistent with a merging system or a bipolar outflow?

Both observations and simulations have shown that gaseous disks are almost always completely destroyed in equal mass mergers[7-9]. Hence, if J2135-0102 is in the intermediate or late stages of a merger, we would expect the kinematics to be strongly disturbed. Instead, we see a relatively smooth rotation profile across the long axis of the galaxy with line widths peaking near the galaxy center, as predicted in simple models of rotating disks. We note that simulations of equal mass mergers at high redshift suggest that with inadequate angular resolution (~0.5-1.0" FWHM), the velocity distortions induced by a merger event may be smeared out giving the appearance of an undisturbed velocity field[9]; however, on the ~150 pc scales probed by the OSIRIS observations of J2135-0102, the simulations suggest that such substructure should be readily apparent in the velocity field.

Alternatively, it is possible that the system is in the early stages of a merger. In this scenario, component 2 is seen in projection with a line-of-sight velocity coincident with the extrapolation of the rotation curve of component 1. Assuming that all velocity vectors are equally probable for the component 2, we derive a <1% probability that the relative spatial position and radial velocity of the component would lie within 10 km/s from component 1 and ±15 degrees from its location on the major axis defined in Figure 2. We therefore view this interpretation as unlikely.

We also consider whether the dynamics could be explained due to an outflow from the central source. While we do expect strong superwinds in J2135-0102, the outflow velocity suggested by the offset between the interstellar absorption features (400±100 km/s)[1] is several times larger than the velocity gradient seen in [OIII] and Hβ (~100 km/s).

Furthermore, for a typical starburst galaxy in the local universe only 3-4% of the Hα luminosity arises from shock-heated gas[10]. This emission also has a much lower surface brightness and is likely difficult to recover at high-redshift. Recalling that Hβ shows the same velocity structure as [O III], these observations suggest that the Hβ and [OIII] luminosity are dominated by radiative processes associated with star formation and not shocks generated in the outflow.

The Rotating Disk Model: In order further evaluate the nature of the velocity field, we explore exponential disk models. We construct simplified two dimensional velocity fields assuming that the velocity follows an arctan function[11]. We allow the peak rotational velocity (v_c), turn-over radius (r_{peak}), inclination angle (i), and position angle (θ) to vary. For each disk model, we construct a datacube with the same pixel scale as our observations and add a Gaussian emission line with line centroid and width reflecting the local dynamics. At each pixel we also add noise appropriate for our data and then refit the velocity field using the same χ^2 minimization line fitting code. We find that the best fit model has a position angle +10º clockwise from the Δy-axis, $v_c \; sin \; i$ = 54.7 km/s, r_{peak}=300pc (Supplementary Figure 2). In Fig. 2c we show the two dimensional velocity field of J2135-0102 and overlay the contours from the best model fit. As can be seen, the model provides a reasonable fit to the data, with the contours tracing the global velocity field, as shown by the one dimensional extracted rotation curve (solid circles) and corresponding model (solid line). The velocity dispersion map and one-dimensional cut are also well-matched to the model (Fig. 2e).

While this simple disk model provides a reasonably good fit to the data, it is worth noting that we are *not* suggesting J2135-0102 is analogous to the cold, disk galaxies seen in the local universe. Indeed, there are numerous small-scale deviations from the model, most

notably at the location of the gas-rich component (at Δx=1.5 kpc on the right-hand side of Fig. 2), where the extracted rotation curve shows an 8 km/s rise and the velocity dispersion shows evidence of a secondary peak. Such substructure might be explained via a disk instability which has led to rapid star formation in a subregion within J2135-0102 and thereby caused a disruption of the local dynamics. Disturbances to the velocity field and line widths are in fact predicted in simulations of unstable disks[12-14]. We also note that our simple disk model fails to explain the 500 pc offset in the peak of the line width distribution from our adopted galaxy center. This is perhaps not surprising considering that in the timescale required to assemble the observed stellar mass given a star formation rate of 60 solar masses yr^{-1} (~100 Myr), a test particle at a radius of 1 kpc will have only completed ~1-2 orbits of the galaxy at the observed rotational velocity; hence it is likely still in a fairly unrelaxed state.

As discussed in the main paper, the line widths are comparable to the inclination-corrected rotational velocity of the galaxy ($v_c / \sigma_0 = 1.2 \pm 0.10$) suggesting considerable random motions. This could arise in two ways[16]. First, as gas is accreted, disk viscosity may convert gravitational potential energy into random motions. This heating may, however, inhibit the efficient dissipative processes necessary for the formation of the clumps seen in J2135-0102. Perhaps instead, random motions were generated *after* star formation was initiated as a result of the stellar winds and outflows present in this galaxy[17]. Which of these two scenarios plays the dominant heating role can be determined with knowledge of the relative distribution of stars and ionized gas. In the latter scenario, random motions are generated after the burst of star formation causing the ionized material to be extended relative to the distribution of stars. In the former case, the heating occurs before the star formation episode, leading to an equally extended distribution of stars and ionized gas.

High-resolution near-infrared imaging will soon provide the necessary constraints on the stellar distribution of J2135-0102, enabling this test to be conducted.

Metallicity Constraints: Additional data covering the redshifted [O II] 3727 Å emission line doublet was obtained using the SINFONI IFU and its associated Laser Guide Star Adaptive Optics system on the 8.2 metre ESO Very Large Telescope UT4 (Yepun). A 3,600 sec (on source) exposure was secured in photometric conditions in 0.6 arcsec seeing using the same tip-tilt reference star as in the OSIRIS observations. These data offer a 3.2 × 3.2 arcsec field with a sampling of 0.10 arcsec pixel^{-1}. The data have a lower spectral resolution ($\lambda/\Delta\lambda$~1500 at 1.5μm) and (due to the shorter exposure time) poorer signal-to-noise than the OSIRIS data, but cover a wider wavelength range, λ = 1.4 – 2.4 μm. The observations were reduced in a similar manner to that described above using the ESOREX pipeline.

This data allows us to examine the chemical composition using the R_{23} index[18,19] derived from the ratio of [O II], [O III] and Hβ emission. Although each line comprising this index is clearly detected over the entire source, the signal-to-noise is insufficient for a measurement in each spatial pixel. However, the data do allow us to bin the spectra in component 1 and 2 separately for which we measure R_{23} = 4.7 ± 0.8 and 3.8 ± 0.4, respectively.

In deriving metallicities from the R_{23} index, uncertainty arises from the double-valued nature of the calibration. We adopt the calibration based on the upper-branch of this relation, yielding 12 + log(O/H) = 8.6 for the entire galaxy, for two reasons. First, this gives a result that is closer to the median metallicity of a large sample of z~2 UV-selected galaxies measured using the [NII]6583/Hα calibration (12+log(O/H) ~ 8.7)[20] and a smaller

sample of z~3 LBGs measured assuming the upper branch of the R_{23} calibration (12+log(O/H) ~ 8.6)[21]. Secondly, our choice is also more consistent with the stellar mass – metallicity relation established for z~2 LBGs[20] given the inferred stellar mass for J2135-0102[6]. Adopting the upper branch calibration and estimating the excitation parameter via the ratio of [O III] and [O II], we find that the oxygen-phase abundance is ~0.9 solar (12 + log(O/H) ~ 8.6) in both components. The lack of a pronounced metallicity gradient in J2135-0102 is consistent with the interpretation that the galaxy is still in a fairly unrelaxed state, having only been actively forming stars for little over a dynamical time.

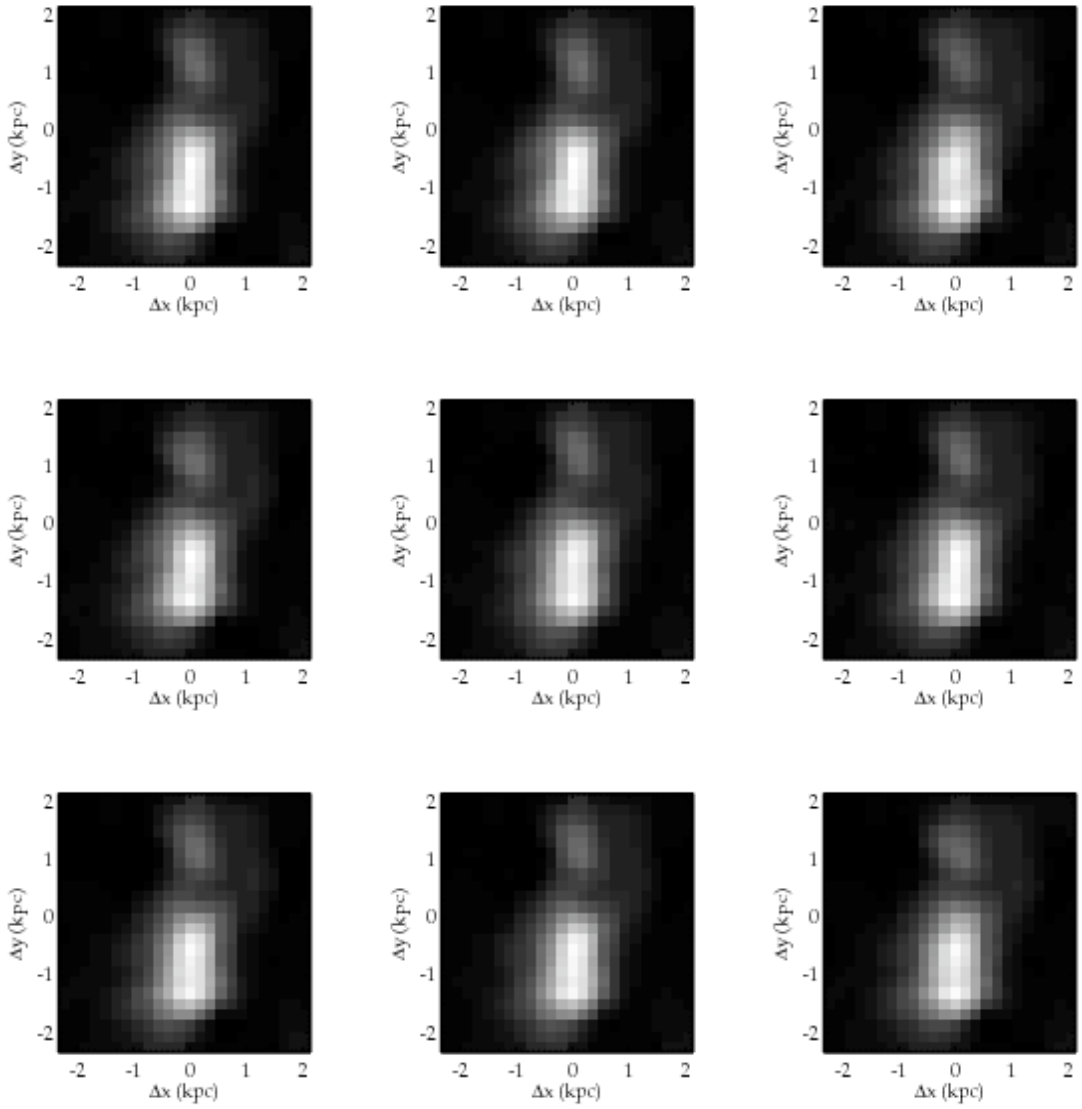

Supplementary Figure 1: Uncertainties in source plane reconstruction. The nine different models are constructed by varying the normalization, elongation, orientation, and external cluster shear of the lens model (see text for details) by $\pm 1\sigma$ from their best-fit values. Ray tracing each of these models and re-deriving the source-plane morphology and velocity field produces only minor changes in the dynamics, typically the various mappings produce a maximum shift of ~0.01

arcseconds compared to the best-fit solution and only a 10% uncertainty in the derived magnification. For consistency with Figure 2, the adaptive source plane grid (with pixel sizes varying between 0.02 and 0.04 arcseconds) is resampled onto a uniform grid with 0.02 arcsecond pixels.

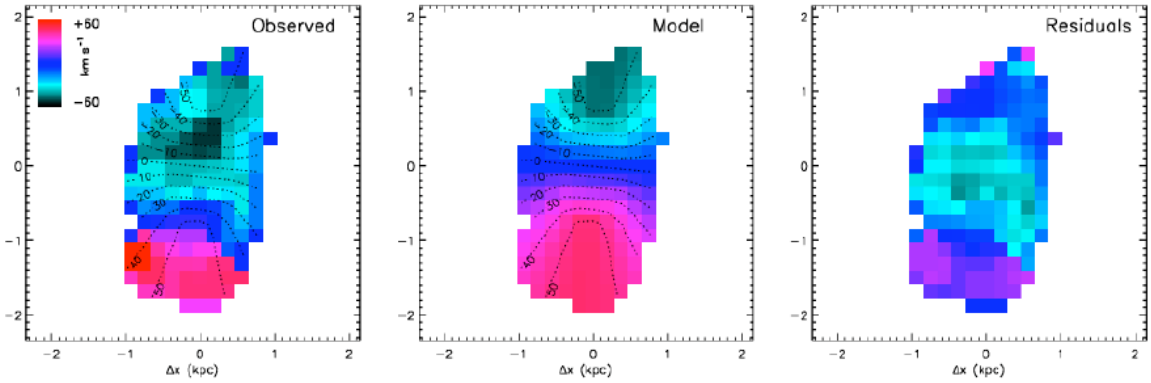

Supplementary Figure 2: Best-fitting disk model and corresponding residuals. The data are fit using a simple arctan function[11] allowing the peak rotational velocity, turn-over radius, inclination angle, and position angle to vary. The model that minimizes χ^2 has θ = +10º clockwise from the Δy-axis, $v_c \, sin \, i$ = 54.7 km/s, i =55º, r_{peak}=300pc. The best-fitting disk model is able to reproduce the velocity shear with reasonably low residuals over most of the velocity field. Regions with larger residuals (<20 km s^{-1}) may potentially reflect substructure within disk, as predicted for unstable disks undergoing rapid star formation[12-14].

Supplementary References:

1. Smail, I., Swinbank, A.M., Richard, J., Ebeling, H., Kneib, J-P, Edge, A.C., Stark, D., Ellis, R.S., Dye, S., Smith, G.P. & Mullis, C., A very bright highly magnified Lyman break galaxy at z=3.07, *Astrophys. J. Lett*., **654**, L33-36 (2007).

2. Larkin, J., Barczys, M., Krabbe, A., et al, OSIRIS: a diffraction limited integral field spectrograph for Keck, *New Astron. Rev*., **50**, 362-364 (2006).

3. Dye, S., Smail, I., Swinbank, A.M., Ebeling, H. & Edge, A.C., Separation of the visible and dark matter in the Einstein ring LBG J213512.73-010143, *Mon. Not. R. astr. Soc.*, **379**, 308- 316 (2007).

4. Dye, S. & Warren, S., Decomposition of the Visible and Dark Matter in the Einstein Ring 0047-2808 By Semilinear Inversion, *Astrophys. J.,* **623**, 31-41 (2005).

5. Kennicutt, R.C., Star Formation along the Hubble Sequence., *Annual Revs. Astron. & Astrophys.,* **36**, 189-232 (1998).

6. Coppin, K.E.K., Swinbank, A.M., Neri, R. et al, A detailed study of gas and star formation in a highly magnified Lyman break galaxy at z=3.07, *Astrophys. J*., **665**, 936-943 (2007).

7. Barnes, J. E. & Hernquist, L., Transformation of Galaxies II: Gas Dynamics in Merging Disk Galaxies. *Astrophys. J.,* **471**, 115-142 (1996).

8. Colina, L., Arribas, S., Monreal-Ibero, A., Kinematics of Low-z Ultraluminous Infrared Galaxies and Implications for Dynamical Mass Derivations in High-z Star-forming Galaxies. *Astrophys. J.,* **621**, 725-737 (2005).

9. Kronberger, T., Kapferer, W., Schindler, S., Ziegler, B.L., 2D Velocity Fields of Simulated Interacting Disc Galaxies, *Astron. & Astrophys.,* **473**, 761-770 (2007).

10. Calzetti, D. *et al.* The Ionized Gas in Local Starburst Galaxies: Global and Small-Scale Feedback from Star-Formation, *Astronom. J.,* **127**, 1405-1430 (2004).

11. Courteau, S., Optical Rotation Curves and Linewidths for Tully-Fisher Applications, *Astronom. J.,* **114**, 2402-2427 (1997).

12. Bournaud, F., Elmegreen, B.G., Elmegreen, D.M., Rapid Formation of Exponential Disks and Bulges at High-Redshift from the Dynamical Evolution of Clump-Cluster Chain Galaxies. *Astrophys. J.* **670**, 237-248 (2007).

13. Bournaud, F. *et al.* Observations and modelling of a clumpy galaxy at z=1.6: Spectroscopic Clues to the Origiin and Evolution of Chain Galaxies. *Astron. & Astrophys. in press,* (2008).

14. Immeli, A. Samland, M., Gerhard, O., Westera, P. Gas physics, disk fragmentation, and bulge formation in young galaxies, *Astron. & Astrophys.,* **413**, 547-561 (2004).

15. Law, D., Steidel, C.C., Erb, D. K., Larkin, J. E., Pettini, M., Shapley, A. & Wright, S., Integral field spectroscopy of high redshift star-forming galaxies with laser-guide star adaptive optics, *Astrophys. J.*, **669**, 929-946 (2007).

16. Forster-Schreiber, N.M., Genzel, R., Eisenhauer, F. et al, SINFONI integral field spectroscopy of z~2 UV-selected galaxies. *Astrophys. J.*, **645**, 1062- 1075 (2006).

17. Thompson, T.A., Quataert, E., Murray, N., Radiation Pressure-supported Starburst Disks and Active Galactic Nucleus Fueling, *Astrophys. J.,* **630**, 167-185 (2005).

18. Pettini, M. & Pagel, B. [O III]/[NII] as an abundance indicator at high redshift, *Mon. Not. R. astro. Soc*., **348**, L59-63 (2004).

19. Pilyugin, L.S. & Thuan, T.X., Oxygen Abundance Determination in H II Regions: The Strong Line Intensities-Abundance Calibration Revisited, *Astrophys.J.*, **631**, 231-243 (2005).

20. Erb, D.K., Shapley, A.E., Pettini, M., Steidel, C.C., Reddy, N., Adelberger, K.L., The Mass Metallicity Relation at z >~ 2, *Astrophys.J.*, **644**, 813-828 (2006).

21. Pettini, M. *et al.* The Rest-Frame Optical Spectra of Lyman Break Galaxies: Star Formation, Extinction, Abundances, and Kinematics. *Astrophys.J.*, **554**, 981-1000 (2001).